PAPER

Analysis of JT-60SA operational scenarios

IOP Publishing | International Atomic Energy Agency Nuclear Fusion

Nucl. Fusion **58** (2018) 026029 (13pp) https://doi.org/10.1088/1741-4326/aa9e15

Analysis of JT-60SA operational scenarios

L. Garzotti[1], E. Barbato[2], J. Garcia[3], N. Hayashi[4], I. Voitsekhovitch[1], G. Giruzzi[3], P. Maget[3], M. Romanelli[1], S. Saarelma[1], R. Stankiewitz[5], M. Yoshida[4] and R. Zagórski[5]

[1] CCFE, Culham Science Centre, Abingdon, Oxon, OX14 3DB, United Kingdom
[2] Unità Tecnica Fusione, ENEA C. R. Frascati,via E. Fermi 45, 00044 Frascati (Roma), Italy
[3] CEA, IRFM, F-13108 Saint Paul Lez Durance, France
[4] National Institutes for Quantum and Radiological Science and Technology, Naka, Ibaraki 311-0193, Japan
[5] Institute of Plasma Physics and Laser Microfusion, Hery 23, 01-497 Warsaw, Poland

E-mail: luca.garzotti@ukaea.uk

Received 7 June 2017, revised 17 November 2017
Accepted for publication 29 November 2017
Published 5 January 2018

Abstract

Reference scenarios for the JT-60SA tokamak have been simulated with one-dimensional transport codes to assess the stationary state of the flat-top phase and provide a profile database for further physics studies (e.g. MHD stability, gyrokinetic analysis) and diagnostics design. The types of scenario considered vary from pulsed standard H-mode to advanced non-inductive steady-state plasmas. In this paper we present the results obtained with the ASTRA, CRONOS, JINTRAC and TOPICS codes equipped with the Bohm/gyro-Bohm, CDBM and GLF23 transport models. The scenarios analysed here are: a standard ELMy H-mode, a hybrid scenario and a non-inductive steady state plasma, with operational parameters from the JT-60SA research plan.

Several simulations of the scenarios under consideration have been performed with the above mentioned codes and transport models. The results from the different codes are in broad agreement and the main plasma parameters generally agree well with the zero dimensional estimates reported previously. The sensitivity of the results to different transport models and, in some cases, to the ELM/pedestal model has been investigated.

Keywords: tokamaks, plasma simulation, transport properties

(Some figures may appear in colour only in the online journal)

1. Introduction

JT-60SA is a tokamak presently under construction in Naka, Japan, using the infrastructure of the existing JT-60 Upgrade experiment. The construction of JT-60SA is a collaboration between Europe and Japan under the broader approach satellite tokamak programme. JT-60SA is designed to support ITER operations and to investigate how to optimise scenarios for future demonstration fusion power plants, which will be built after ITER. The acronym SA stands for 'Super' and 'Advanced', since the tokamak will have superconducting coils and study advanced modes of plasma operation. Further details of its experimental programme are explained in the JT-60SA research plan [1].

The intrinsic flexibility of JT-60SA will allow the study of a variety of scenarios. In particular, the scenarios under consideration for plasma operations on JT-60SA are: pulsed, inductive, standard H-modes, similar to the ITER baseline scenario; advanced inductive, high-β, low magnetic shear scenarios, similar to the ITER hybrid scenario and fully non-inductive, steady-state, advanced scenarios, which could be extrapolated to a steady-state demonstration fusion power plant. The main parameters of the reference scenarios are given in tables 2 and 3 of [1].

The scenarios described above have been developed with the help of the 2-dimensional equilibrium code ACCOME [2] (consistently with current drives) and then assessed by the 0.5-dimensional code METIS [3]. The results have been

extensively reported in [4]. To increase the confidence in these simulations and to further check whether the plasma parameters calculated by ACCOME and METIS are achievable, we have modelled the flat top of the baseline, hybrid and fully non-inductive scenario with more sophisticated 1.5-dimensional transport codes. The aim of this paper, which builds on the model validation performed using selected sets of JT-60U and JET discharges [5], is to report the results of these simulations.

A further motivation for the study presented in this paper was to provide a number of other research activities centred on JT-60SA with a set of simulations of the main operational scenarios as self-consistent as possible. These activities range from the design of diagnostic systems (see, for example, [6]) to the analysis of systems aiming at controlling different aspects of the operational scenarios. As examples of the control schemes described in the JT-60SA research plan we can mention the control of the plasma shape and vertical stability (especially for high β_N and high elongation plasmas), of certain kind of MHD instabilities, like resisting wall modes by means of saddle coils or neoclassical tearing modes by means of electron cyclotron current drive [7], of the density (especially in saturated wall conditions) by means of pellet injection [8] and the power load on the divertor plates (especially in high additional power density scenarios) by means of impurity seeding [9]. Most of these areas of research have already started to make use of the results presented in this paper as input to their modelling activities.

Finally, it should be noted that this paper deals with the flat-top phase of the scenarios analyzed. The results presented here should be regarded both as a confirmation by means of 1.5-dimensional transport codes of the feasibility of the scenarios designed with ACCOME and METIS and as a 'target' for simulations of the front-end of the discharge including the current ramp-up (especially for the hybrid scenario) and the access to H-mode or a starting point for simulations of the discharge termination including the current ramp-down and the H-L transition. These simulations are outside the scope of this paper, but the strategy to approach the problem will be similar to that presented here. Starting from transport models that have been reasonably validated in existing machines for the phase of the discharge of interest and using different assumptions for example for the L-H transition threshold or for the current diffusion model, one should be able to assess whether or not and under which conditions the target parameters of a given scenario are achievable and devise a safe strategy to terminate the discharge. An example of this approach can be found in [10, 11] where simulations performed with the JINTRAC suite of codes of the ITER baseline scenario, including current ramp-up and ramp-down, are presented.

The structure of the paper is the following: in section 2 we give a general description of the codes and the transport models deployed in this study and of the simulation conditions; in section 3 we describe the results for the baseline H-mode scenario; in section 4 we present the results for the hybrid scenario; in section 5 we describe the results for the advanced steady-state scenario; in section 6 we discuss the results obtained and in section 7 we summarize the main conclusions of the study.

2. Description of the simulations

The transport codes used in the simulations presented in this study were: ASTRA [12], CRONOS [13], JINTRAC [14] and TOPICS [15]. Each transport code is equipped with a number of core transport models. In particular, for the analysis presented in this paper, we used: the physics-based transport models GLF23 [16] (implemented in ASTRA, CRONOS and TOPICS) and CDBM [17] (implemented in CRONOS, JINTRAC and TOPICS) and the semi-empirical transport model Bohm/gyro-Bohm [18] (implemented in ASTRA and JINTRAC).

All transport models have been validated in the past on JET and JT-60U for the scenarios considered in this study [5, 18, 19] and, since the operational regime of JT-60SA is largely similar to those of JET and JT-60U, we considered legitimate the extrapolation of these models to the new machine. The main limitation of the models used in this study is due to the fact that they do not capture the effects of the fast particle population on transport and this could limit the validity of the extrapolation to the fully non-inductive steady-state scenario. Nevertheless, as we shall see in the rest of the paper, using different codes and transport models for the same scenario gives a reasonable interval in which the expected performance of JT-60SA should lie.

We deliberately chose not to use more complex transport models like, for example, TGLF [20] or QuaLiKiZ [21] because, at the time when this study was performed, their implementation in the codes at our disposal was not mature enough to perform extensive simulations of JET, JT-60U and JT-60SA scenarios. Moreover, the computational burden associated with these transport models is too heavy for the time scale of the simulations presented here, which is comparable with the current diffusion time. Nevertheless, some of the physics captured by this more complex models is taken into account by the older physics-based model GLF23.

In all simulations we solve transport equations for the current density and the ion and electron temperature. In CRONOS and JINTRAC, the equation for the ion density is also solved and the electron density is obtained from prescribed Z_{eff} profiles and impurity mix, whereas in ASTRA and TOPICS the electron density profiles are prescribed and taken from the ACCOME reference results. Modelling of plasma rotation was included only in the JINTRAC simulations for the advanced steady-state scenario to compare the prediction of different models for the formation of an internal transport barrier (ITB).

Simulating an H-mode plasma requires a model to describe the edge transport barrier (ETB), where the physics governing the transport is much less understood than in the core and the transport is intermittent due to the presence of ELMs. The codes used in this study adopt different approximations to treat this problem. In ASTRA and TOPICS the problem is avoided by imposing the boundary conditions at the top of the ETB and not solving the transport equations inside it, whereas in CRONOS and JINTRAC simulations the boundary conditions are imposed at the separatrix. In particular, in TOPICS, the electron and ion temperature profiles in the pedestal are determined on the basis of an

EPED1 pedestal width scaling [22] and a stability check by the linear MHD code MARG2D [23].

In JINTRAC, the transport in the ETB can be determined in two ways. The first is to adopt the continuous ELM model described in [24], which mimics the limiting effect of the ELMs on the pressure gradient in the ETB by introducing additional transport averaged over time and clamps the normalized pressure gradient in the ETB α at a prescribed critical value α_c. The second is to directly prescribe the particle diffusivity D and the ion and electron thermal conductivity $\chi_{i,e}$ in the pedestal to obtain the desired density and temperature pedestal height. In both cases the width of the pedestal is prescribed as a free input parameter.

In CRONOS, the pedestal energy content is estimated by means of the Cordey two-term scaling [25], the height of the density and temperature pedestal is then calculated by imposing neoclassical transport in the ETB, whereas the pedestal width is obtained from the EPED1 model and turns out to be proportional to $\sqrt{\beta_p}$ [22], where the pedestal pressure was self-consistently calculated using the Cordey scaling.

The particle source due to the gas puff and the ionization of the neutral atoms recycling at the wall is described in JINTRAC by FRANTIC [26], where a ray tracing technique is used to calculate the neutral density inside the plasma in cylindrical geometry taking into account ionization and multiple charge exchange processes to determine the profile of the ionization particle source. In CRONOS a Gaussian profile was assumed for the ionization source, the shape of which was tuned against JET and JT-60U data and kept the same in JT-60SA extrapolations [5].

Impurities are treated in a simplified way in all codes. In particular, since JT-60SA first wall will be made of C at least for the first phase of the machine life, C is assumed to be the dominant impurity and its concentration is determined from the prescribed value of Z_{eff} and the assumption that it is completely ionized. The impurity density profile obtained in this way is kept constant during the simulation as impurity transport is not addressed in this study. Indeed, some integrated core/SOL simulations of the expected impurity dynamics in JT-60SA were done with COREDIV and presented in [27]. It should be noted that these COREDIV simulations adopted a simplified description of the core transport with respect to the simulations presented in this study. It is also worth noting that, for some cases presented in this paper, we modified slightly the value of Z_{eff} with respect to the initial value common to all codes to bring the simulation more in line with the COREDIV results, however this did not changed significantly the 0-dimensional parameters of the scenarios.

For the simulations presented in this paper, the power deposition associated with additional heating was calculated in CRONOS by means of the codes NEMO/SPOT [28] for the positive and negative neutral beam injection (NBI) heating and REMA [29] for the electron cyclotron resonance heating (ECRH). The same heat source profiles were then used in ASTRA. In JINTRAC the NBI power deposition was modelled by PENCIL [30], whereas the ECRH power deposition was assumed equal to the one used in the CRONOS and ASTRA simulations. As a consequence, in ASTRA and JINTRAC, the heat deposition profiles are not completely consistent with the final equilibrium density and temperature profiles. In TOPICS, the NBI power deposition heating is calculated with a Fokker-Planck model [31] and the NBI-driven current is calculated using Mikkelsen and Singer's approximation [32]. The EC heating and current drive are computed with the EC code described in [33].

The 2-dimensional equilibria for the transport simulations are provided by different equilibrium codes. ASTRA can use either SPIDER [34, 35] or a three-moment representation of the equilibrium, CRONOS uses HELENA [36] as its standard equilibrium solver, JINTRAC calculates the equilibrium with the ESCO solver [37] and TOPICS uses the free-boundary equilibrium code described in [38].

Finally, sawteeth are taken into account in all codes either by means of the Kadomstev model [39] (ASTRA, JINTRAC and TOPICS) or a simpler continuous sawtooth model (CRONOS) whereby D and $\chi_{i,e}$ are increased (typically to values between 0.3 and 0.4 m^2s^{-1}) inside the $q = 1$ surface to flatten the density and temperature profiles and the value of the plasma resistivity at the $q = 1$ surface is extended inside this region to reduce the current density in the plasma core and, consequently, increase q and the flux consumption. When the Kadomstev model is used, the period of the sawteeth is prescribed and is of the order of a few hundreds of milliseconds. Other kinds of MHD activity (like, for example, neoclassical tearing modes) are not taken into account in the simulations presented in this paper.

In the study presented in the following section we took as initial condition for the transport simulations the profiles obtained from METIS runs [3] and we run ASTRA, CRONOS and JINTRAC for several confinement times ($\geqslant 10$ s) in order to reach equilibrium. TOPICS simulations were run in a similar way but starting from ACCOME results as initial condition. We then compared the 0-dimensional parameter derived from the 1.5-dimensional transport runs and the radial density, temperature and q profiles with the reference parameters and between the different codes. This allowed us to assess the consistency of the reference parameters and of the METIS/ACCOME analysis with more sophisticated transport models and the robustness of the result with respect to the variation of the profiles due to the use of different transport models.

3. Baseline H-mode scenario

The first scenario analysed is a standard H-mode similar to the ITER baseline scenario (referred to as scenario 2 in the JT-60SA research plan). For this scenario $B_T = 2.25$ T, $I_p = 5.5$ MA, $P_{NBI} \approx 34$ MW (10 MW negative NBI and 24 MW positive NBI) and $P_{ECRH} = 7$ MW. The plasma boundary used in the simulations is shown in figure 1.

The boundary conditions on the density and temperature profiles for the simulations of scenario 2 were chosen to match as closely as possible the results of integrated core/SOL simulations with the COREDIV code [27]. It should be noted, however, that, because of the different ways impurities are treated in different codes, it was not possible to match exactly

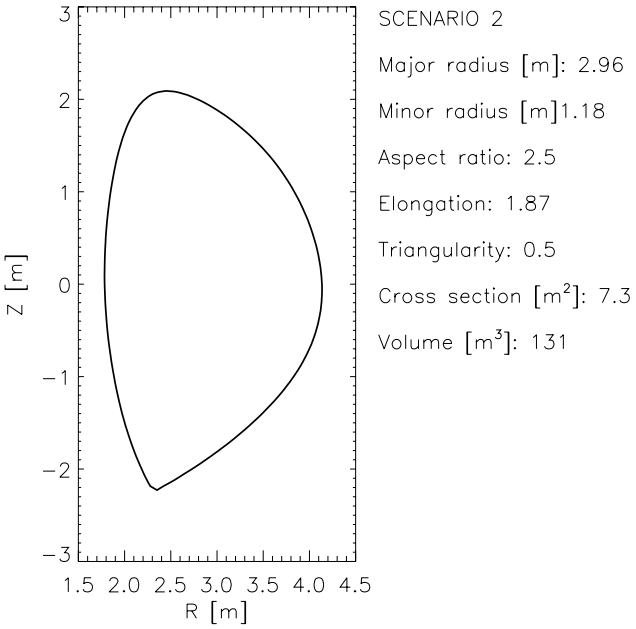

Figure 1. Plasma boundary and main geometrical parameters used in the simulation of a JT-60SA H-mode plasma (scenario 2).

the values obtained by COREDIV. Nevertheless, we found that values of $n_e = 2.3 \cdot 10^{19}$ m^{-3} and $T_e = T_i = 150$ eV at the separatrix imply a sputtering rate of impurities (mainly C) from the divertor compatible with the assumption $Z_{eff} = 1.8$.

As described in [5], based on the validation of different transport models on specific JET and JT-60U shots, CRONOS simulations use GLF23 for particle and heat transport respectively, whereas TOPICS simulations are limited to heat transport with GLF23. On the other hand, ASTRA and JINTRAC use the semi-empirical Bohm/gyro-Bohm transport model, which has been extensively validated on JET.

The equilibrium electron density and electron and ion temperatures profiles obtained with ASTRA, CRONOS, JINTRAC and TOPICS are shown in figure 2, whereas the current density profiles are shown in figure 3. To obtain the same electron density and electron and ion temperature at the top of the pedestal in CRONOS and JINTRAC we prescribed in JINTRAC $D = 0.2$ m^2 s^{-1} and $\chi_{i,e} = 0.2$ m^2 s^{-1} inside the ETB. It is worth noting that, in these simulations, the value of α, the normalized pressure gradient inside the pedestal, was $\sim$2, which is somehow higher than what is observed, for example, on JET and could be beyond the peeling-ballooning stability boundary. These results highlight the importance of having a reliable prediction for the height and width of the density and temperature pedestal and of checking the assumptions made on the pedestal against ballooning stability criteria.

ASTRA gives results broadly in line with CRONOS and JINTRAC, whereas TOPICS predicts the flattening of the ion and electron temperature profile outside $\rho \approx 0.3$. This is because the prescribed density profile features a fairly steep gradient at $\rho \approx 0.5$, which destabilizes the trapped electron modes (TEMs) and results in large diffusivities at this radial position and a shallow ion and electron temperature gradient. TEMs can be stabilized by $E \times B$ flow shear, which in JT-60SA can be significant because of the degree of toroidal rotation control achievable thanks to the large amount and the flexibility of the NBI power available. Since the rotation profiles have not been simulated and tested for this scenario, in order to verify the TOPICS results, TOPICS was also used with the CDBM and Bohm/gyro-Bohm transport models. These models, with no or little effect of the $E \times B$ flow shear, showed less good agreement with the JET/JT-60U experimental data than GLF23 [5] and predict smoother profiles with almost the same 0-dimensional parameters.

The 0-dimensional parameters derived from these simulations are summarized in table 1 where the reference values (obtained from ACCOME) from the research plan [1] are also reported for comparison. It can be seen that, despite the differences in the density and temperature profiles predicted by the different codes, in general all codes give values for 0-dimensional quantities close to the reference ones.

4. Hybrid scenario

The second scenario simulated in this study is an advanced inductive scenario similar to the ITER hybrid scenario (referred to as scenario 4.2 in the JT-60SA research plan). For this scenario $B_T = 2.28$ T, $I_p = 3.5$ MA, $P_{NBI} \approx 30$ MW (10 MW negative NBI and 20 MW positive NBI) and $P_{ECRH} = 7$ MW. The plasma boundary used in the simulations is shown in figure 4.

Also in this case we prescribed the boundary conditions on the density and temperature profiles on the basis of integrated core/SOL simulations with the COREDIV code, which indicate that $n_e = 1.4 \cdot 10^{19}$ m^{-3} and $T_e = T_i = 100$ eV at the separatrix lead to a sputtering rate of impurities from the divertor compatible with the assumption $Z_{eff} = 2.1$.

Fully predictive JINTRAC simulations for scenario 4.2 were performed with the Bohm/gyro-Bohm transport model assuming a value for $\alpha_c = 1.5$ in the ETB.

Semi-predictive ASTRA simulations (i.e. simulations where we solved the equations for the ion and electron temperature profiles whereas the density profile was prescribed) were performed for this scenario with the semi-empirical Bohm/gyro-Bohm and the physics-based GLF23 transport models.

Finally, fully predictive CRONOS simulations similar to scenario 2 were performed with the GLF23 transport model for the density equation and the CDBM transport model for the ion and electron temperature equations. This particular choice of transport models was based on the analysis of hybrid plasmas on JET and JT-60U described in [5], where it was shown that, for this particular scenario, GLF23 was more successful in simulating the plasma density whereas CDBM did a better job at reproducing the electron and ion temperature profiles.

As previously done for scenario 2, the 0-dimensional parameters derived from these simulations are summarized in table 2 where the values from the research plan are also reported for comparison. It can be seen that, despite the even greater differences with respect to scenario 2 in the density and temperature profiles predicted by the different codes, also

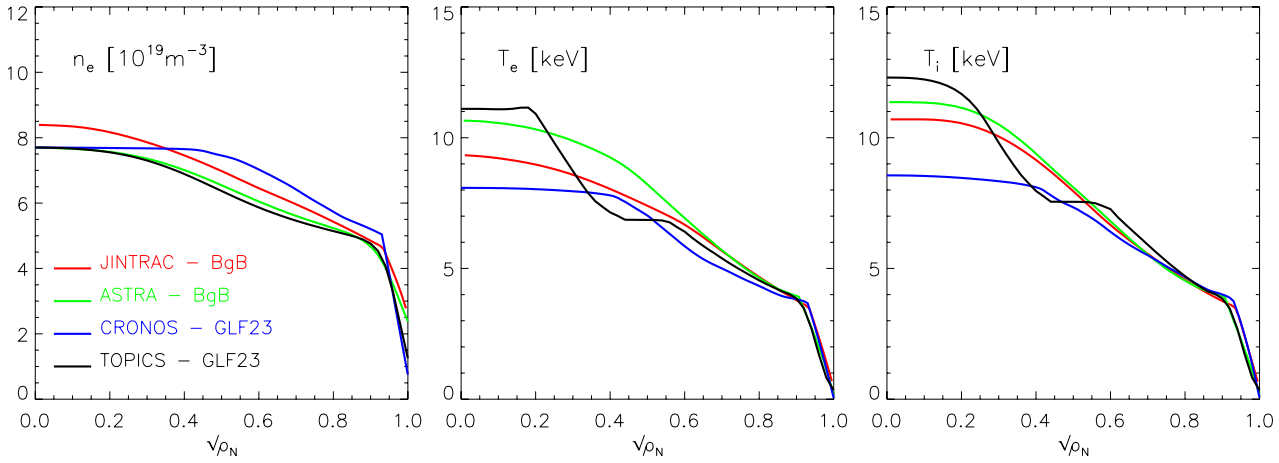

Figure 2. Predicted electron density, electron temperature and ion temperature profiles for a JT-60SA H-mode plasma (scenario 2). The codes and the transport models used in the simulations are indicated in the legend.

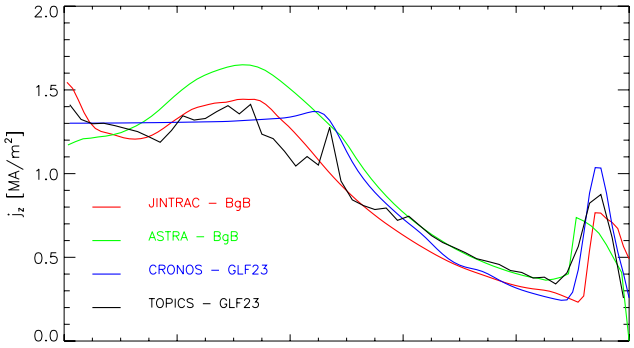

Figure 3. Predicted total current density profiles for a JT-60SA H-mode plasma (scenario 2). The codes and the transport models used in the simulations are indicated in the legend.

Table 1. Reference 0-dimensional parameter for scenario 2 compared with the values obtained from the 1.5-dimensional transport simulations described in the paper.

Scenario 2	ASTRA	CRONOS	JINTRAC	TOPICS	Reference
B_T (T)	2.25	2.25	2.25	2.25	2.25
I_p (MA)	5.5	5.5	5.5	5.5	5.5
f_{bs} (%)	25	28	34	29	28
f_{ni} (%)	40	39	46	51	50
q_{95}	2.8	3.0	3.5	3.1	3.0
P_{NBI} (MW)	32.9	33.0	33.0	34.0	34.0
P_{ECRH} (MW)	7.0	7.0	7.0	7.0	7.0
n_{e0} (10^{19} m^{-3})	7.7	7.5	8.2	7.7	7.7
$\langle n_e \rangle$ (10^{19} m^{-3})	5.8	6.2	5.1	5.6	5.6
T_{e0} (keV)	10.7	8.1	10.3	11.1	13.5
$\langle T_e \rangle$ (keV)	6.3	5.4	7.2	5.8	6.3
T_{i0} (keV)	11.5	8.5	12.4	12.3	13.5
$\langle T_i \rangle$ (keV)	6.3	5.8	6.5	6.3	6.3
W_{th} (MJ)	22.8	22.5	23.0	21.2	22.0
H_{98}	1.2	1.1	1.2	1.2	1.3
β_N	3.0	3.0	3.1	2.9	3.1
τ_E (s)	0.58	0.61	0.60	0.52	0.64
Z_{eff}	1.8	1.8	1.8	2.0	—

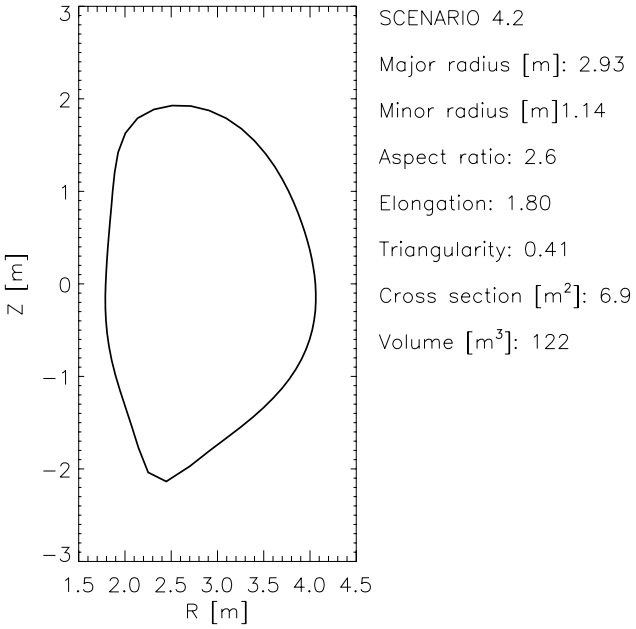

Figure 4. Plasma boundary and main geometrical parameters used in the simulation of a JT-60SA hybrid plasma (scenario 4.2).

in this case in general all codes give values for 0-dimensional quantities close to the reference ones.

The equilibrium electron density and electron and ion temperatures profiles and the q profiles obtained with ASTRA, CRONOS and JINTRAC are plotted in figures 5 and 6 respectively and deserve some comments.

First of all, we note that all codes and transport models predict or assume similar values for the height and width of the density and temperature pedestal, with the exception of ASTRA with the Bohm/gyro-Bohm transport model, where the electron temperature at the top of the ETB does not evolve and is fixed at the beginning of the simulation at a value ∼30% lower than the one attained by the other codes, and JINTRAC with the Bohm/

Table 2. Reference 0-dimensional parameter for scenario 4.2 compared with the values obtained from the 1.5-dimensional transport simulations described in the paper.

Scenario 4.2	ASTRA BgB / GLF23	CRONOS	JINTRAC	Reference
B_T (T)	2.28 / 2.28	2.28	2.28	2.28
I_p (MA)	3.5 / 3.5	3.5	3.5	3.5
f_{bs} (%)	51 / 43	40	48	40
f_{ni} (%)	79 / 75	66	77	58
q_{95}	4.7 / 4.7	4.6	4.6	4.4
P_{NBI} (MW)	29 / 32	29	29	30
P_{ECRH} (MW)	7.0 / 7.0	7.0	6.8	7.0
n_{e0} (10^{19} m^{-3})	7.9 / 7.9	8 6	6.4	8.4
$\langle n_e \rangle$ (10^{19} m^{-3})	5.0 / 5.0	5.0	4.7	6.2
T_{e0} (keV)	7.8 / 10.0	8.2	9.7	7.5
$\langle T_e \rangle$ (keV)	4.0 / 3.6	3.8	5.2	3.7
T_{i0} (keV)	8.7 / 13.0	9.0	11.3	7.5
$\langle T_i \rangle$ (keV)	4.1 / 4.3	4.3	4.6	3.7
W_{th} (MJ)	12.6 / 13.4	12.5	14.2	13.4
H_{98}	1.3 / 1.3	1.3	1.3	1.2
β_N	3.0 / 3.2	3.2	3.4	3.0
τ_E (s)	0.35 / 0.40	0.40	0.40	0.42
Z_{eff}	1.7 / 1.7	2.1	2.1	—

gyro-Bohm transport model which predicts an ion temperature at the top of the ETB ∼30% lower than the other codes.

Secondly, we can see that JINTRAC equipped with the Bohm/gyro-Bohm transport model predicts a density profile significantly less peaked than CRONOS with GLF23.

Thirdly, we should note that the rather sharp peak on the electron and ion temperature profile inside $\rho = 0.1$ predicted by ASTRA with GLF23 is due to the fact that this model tends to predict no instabilities near the plasma axis and therefore almost no transport in this region. This is probably unphysical and the electron and ion temperature profiles are expected to be flatter near the magnetic axis because of some residual transport not accounted for by GLF23.

Finally, we can observe the presence of an ITB on the electron and ion temperature profiles predicted by the CRONOS with the CDBM transport model. This is due to the tendency of CDBM to suppress the heat conductivity and develop ITBs in regions of the plasma with low shear and strong pressure gradients.

These differences in density and temperature profiles are responsible for the differences in the predicted q profiles. The hollowness of the q profile predicted by JINTRAC is due mainly to the flatter density gradient driving less bootstrap current in the plasma centre, whereas the low q_0 predicted by ASTRA with the GLF23 transport model is a consequence of the sharp peak on the electron temperature profile resulting in a more peaked inductive current density profile.

5. Steady-state scenario

The third scenario simulated is an advanced steady-state scenario (referred to as scenario 5.1 in the research plan). This scenario is based on the results of experiments performed on JET and JT-60U aiming at establishing plasmas with an ITB driving a significant fraction of the bootstrap current. A description of the main characteristics and of the modelling of these experiments can be found in [19] and references within.

In this study we analysed two versions of this scenario. A 'high power' version with $B_T = 1.72$ T, $I_p = 2.3$ MA, $P_{NBI} \approx 30$ MW (10 MW negative NBI and 20 MW positive NBI) and $P_{ECRH} = 7$ MW and a 'low power' version, more conservative from the point of view of MHD stability, with $B_T = 1.72$ T, $I_p = 2.3$ MA, $P_{NBI} \approx 17$ MW (5 MW negative NBI and 12 MW positive NBI) and $P_{ECRH} = 7$ MW. The plasma boundary used in the simulations is shown in figure 7.

Once again, we prescribed the boundary conditions on the density and temperature profiles for the simulations on the basis of integrated core/SOL simulations with the COREDIV code, which indicate that $n_e = 1.3 \cdot 10^{19}$ m^{-3} and $T_e = T_i = 50$ eV at the separatrix lead to a sputtering rate of impurities from the divertor compatible with the assumption $Z_{eff} = 1.7$. It is worth noting that in the JINTRAC simulations presented in this section the boundary condition on the current density profile was imposed not by prescribing the total plasma current, as in the simulations for the standard H-mode and advanced inductive scenarios, but by prescribing a value of the loop voltage of a few mV (typically in the range between 1 and 2 mV).

Two important points make this scenario particularly difficult to simulate: the sensitivity of the q profile to the non-inductive current drive and the possible formation of an ITB, which in turn could generate a significant amount of bootstrap current. We have investigated these questions in both the 'high power' and 'low power' versions of the scenario and the results are reported in sections 5.1 and 5.2 respectively.

5.1. Steady-state H-mode scenario: 'high power' version

For the analysis of the 'high power' version of the scenario we performed three JINTRAC runs with prescribed D and $\chi_{i,e}$ in the ETB to obtain width and height of the density and temperature pedestal similar to those calculated by CRONOS and corresponding to $\alpha_c \sim 1.5$. It should be noted that this value for α_c is lower than the typical values observed, for example, on JET.

The first two simulations used the Bohm/gyro-Bohm transport model complemented with the assumption $\chi_\phi = \chi_i$ for the momentum transport (equivalent to the assumption that the Prandtl number Pr is equal to one across the whole plasma) and a criterion for the formation of an ITB [40], which takes into account the magnetic shear s and the ratio $\omega_{E\times B}/\gamma$ between the shear of the $E \times B$ velocity and a parameter γ, which has the physical dimensions of a growth rate. The expression used in JINTRAC for γ has the simplified form $\gamma = v_{th,i}/R$, where $v_{th,i}$ is the ion thermal velocity and R is the plasma major radius. This expression is of a heuristic nature and captures well the ion temperature dependence of the ITB threshold in JET. In particular, it has been shown in [40] on a statistical basis that an ITB is formed when the condition $z = -0.14 + s - 1.47\omega_{E\times B}/\gamma < 0$ is satisfied. Therefore, the Bohm term in the expression for D and $\chi_{i,e}$ in the mixed Bohm/gyro-Bohm transport model is multiplied by $\Theta(z)$, where Θ is the Heaviside step function. Here it should be stressed that, given the statistical nature of this model and

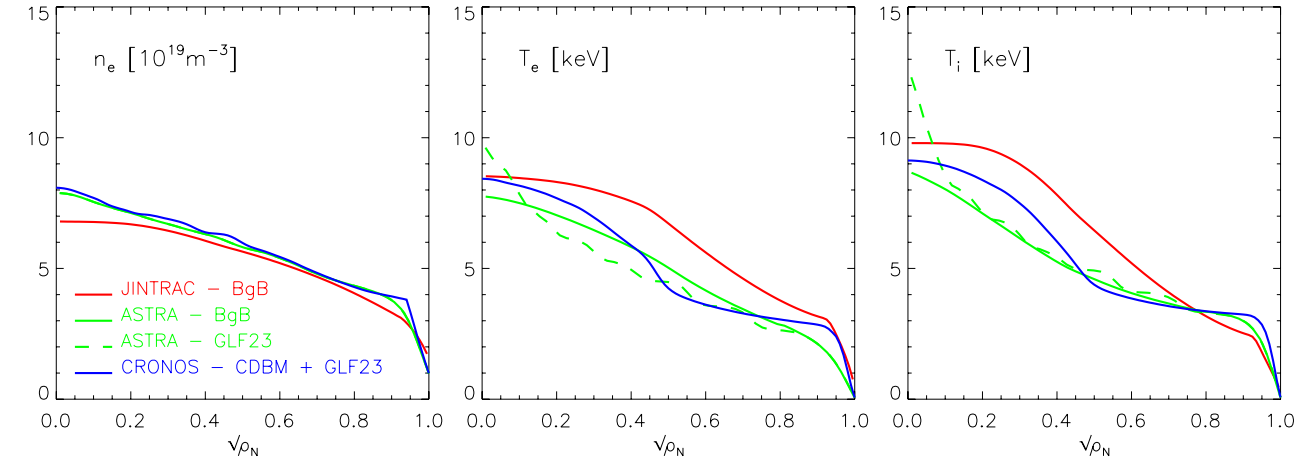

Figure 5. Predicted electron density, electron temperature and ion temperature profiles for a JT-60SA hybrid plasma (scenario 4.2). The codes and the transport models used in the simulations are indicated in the legend.

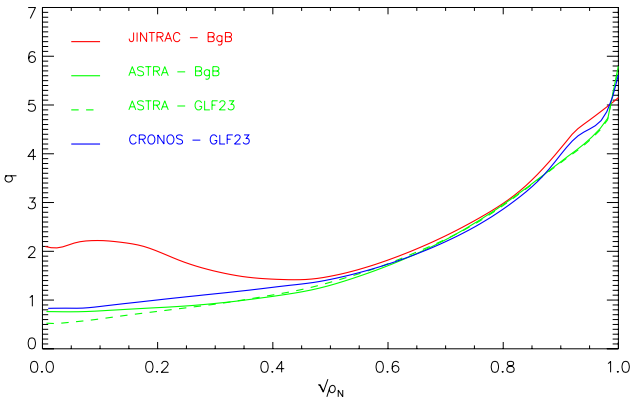

Figure 6. Predicted q profiles for a JT-60SA hybrid plasma (scenario 4.2). The codes and the transport models used in the simulations are indicated in the legend.

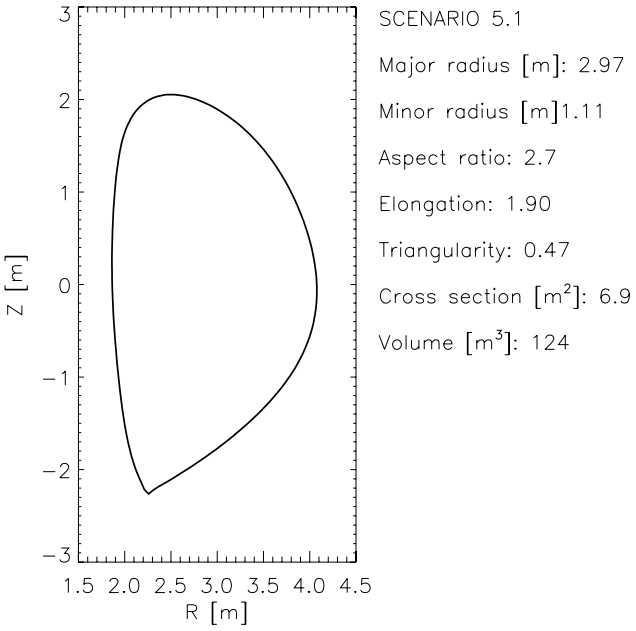

Figure 7. Plasma boundary and main geometrical parameters used in the simulation of a JT-60SA advanced steady-state plasma (scenario 5.1).

the fact that the regression rule was tuned on a database of JET plasmas, one should be careful when extrapolating the model to a different machine.

In one simulation, the power deposition, current drive and torque profile associated with the beam injection were prescribed accordingly to the NEMO/SPOT calculation for a CRONOS simulation of the same scenario (and, as a consequence, were not self-consistent with the density and temperature profiles predicted by JINTRAC), whereas in the other two they were calculated self-consistently by PENCIL inside JINTRAC. In the first case (NEMO/SPOT) the current driven by the NBI was 0.9 MA and in the second (PENCIL) 0.8 MA. A Gaussian shape centred at $\rho = 0.4$ for the current density associated with electron cyclotron current drive (ECCD) profile was prescribed in both simulation and the total ECCD-driven current was $\leqslant 150$ kA, a negligible fraction of the total plasma current.

The third JINTRAC simulation used the CDBM transport model and the NBI power deposition, current drive and torque profile calculated by PENCIL. In this case the NBI driven current was 0.9 MA. In this way we were able to test the sensitivity of the ITB formation to the transport model and of the q profile to the details of the beam power deposition, current drive and torque profile.

The results are summarized in figures 8–11. In figures 8–10 we show the total current density profile, the neutral beam-driven, the electron cyclotron-driven and the bootstrap current density for the three cases. Unsurprisingly, the shape of the q profile is very sensitive to the on-axis current density. PENCIL predicts less on-axis current density and a significantly hollow q profile, whereas NEMO/SPOT predicts a higher on-axis density and less strongly reversed q profile. This might be due to the fact that PENCIL does not take into account the finite size of the fast ion orbits, whereas NEMO/SPOT does and therefore allows for the beam fast ions deposited off-axis to reach the centre of the plasma and contribute to the on-axis current drive. Moreover, as explained above, the NEMO/SPOT calculation were not done self-consistently with the density and temperature profiles calculated by JINTRAC and therefore, because of the sensitivity of the deposition profiles

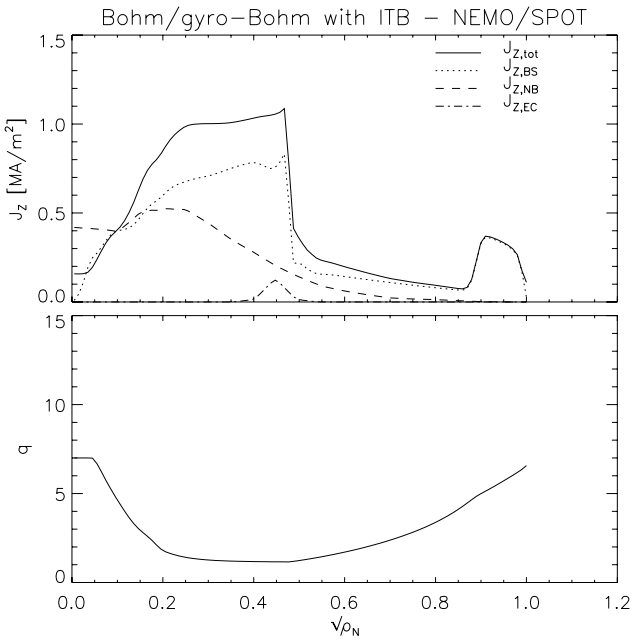

Figure 8. Total current density j_z, neutral beam-driven current density $j_{z,\mathrm{NB}}$, bootstrap current density $j_{z,\mathrm{BS}}$, electron cyclotron driven current density $j_{z,\mathrm{EC}}$ and safety factor q profiles for a JT-60SA advanced steady-state plasma (scenario 5.1 'high power' version). The transport model used in the simulation is the Bohm/gyro-Bohm transport model and the neutral beam-driven current density is calculated with NEMO/SPOT (not self-consistently).

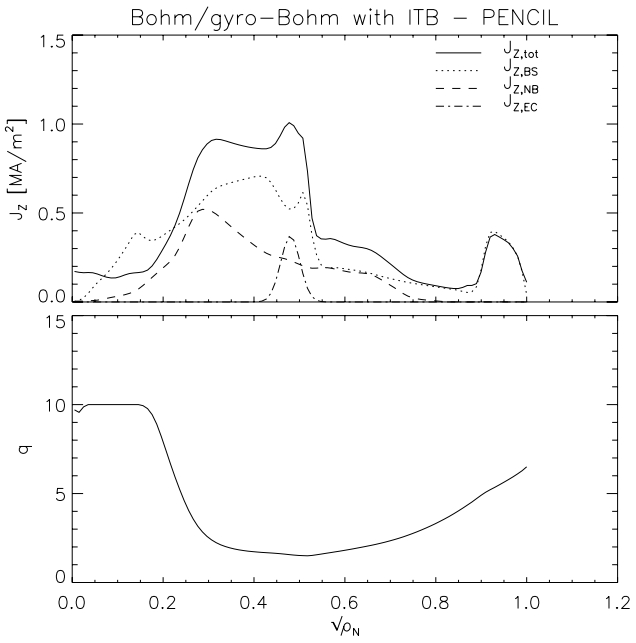

Figure 9. Total current density j_z, neutral beam-driven current density $j_{z,\mathrm{NB}}$, bootstrap current density $j_{z,\mathrm{BS}}$, electron cyclotron driven current density $j_{z,\mathrm{EC}}$ and safety factor q profiles for a JT-60SA advanced steady-state plasma (scenario 5.1 'high power' version). The code used in the simulation is JINTRAC with the Bohm/gyro-Bohm transport model and the neutral beam-driven current density is self-consistently calculated with PENCIL.

to these quantities, this fact could be another source of discrepancy between the simulations.

It is worth noting that the hollow q profiles produced by the markedly off-axis neutral beam-driven current density profile predicted by PENCIL make the calculation of the equilibrium numerically difficult. In some cases a small amount of current on axis had to be added to help clamp the value of q on axis. In fact, the simulations performed using PENCIL could only be extended for 15–20 s and had to be stopped before the current density profile was completely relaxed. However, this time is much longer than the confinement time and therefore the kinetic profiles could relax almost to a complete stationary state.

As for the density and temperature profiles, figure 11 shows that all three JINTRAC runs predict the formation of an ITB at $\rho = 0.45$. From figure 11, we can also see that these results are in line with the CRONOS simulation using the GLF23 transport model for the density and the CDBM transport model for the ion and electron temperature. The differences in the strength and the position of the ITB in different simulations can be attributed to the fact that the formation of an ITB in CDBM is very sensitive to the details of the gradient of the pressure profile and to the local shear. Therefore, small differences in the pressure or the q profile between two runs can result in different ITBs.

In figure 11, we compare the JINTRAC and CRONOS results with an ASTRA simulation of the same scenario using a three-moment equilibrium and the Bohm/gyro-Bohm transport model, but without any prescription for the formation of an ITB. In this case the absence of an ITB results in a lower

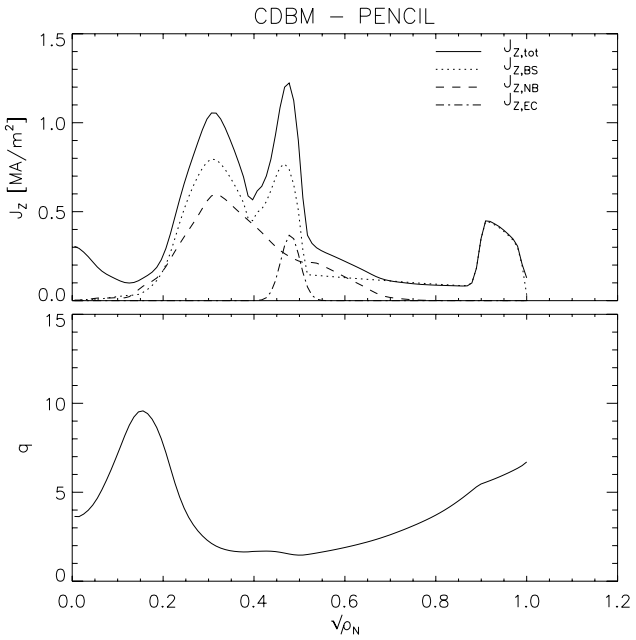

Figure 10. Total current density j_z, neutral beam-driven current density $j_{z,\mathrm{NB}}$, bootstrap current density $j_{z,\mathrm{BS}}$, electron cyclotron driven current density $j_{z,\mathrm{EC}}$ and safety factor q profiles for a JT-60SA advanced steady-state plasma (scenario 5.1 'high power' version). The code used in the simulation is JINTRAC with the CDBM transport model and the neutral beam-driven current density is self-consistently calculated with PENCIL.

energy content and in ion and electron temperature lower than in JINTRAC and CRONOS.

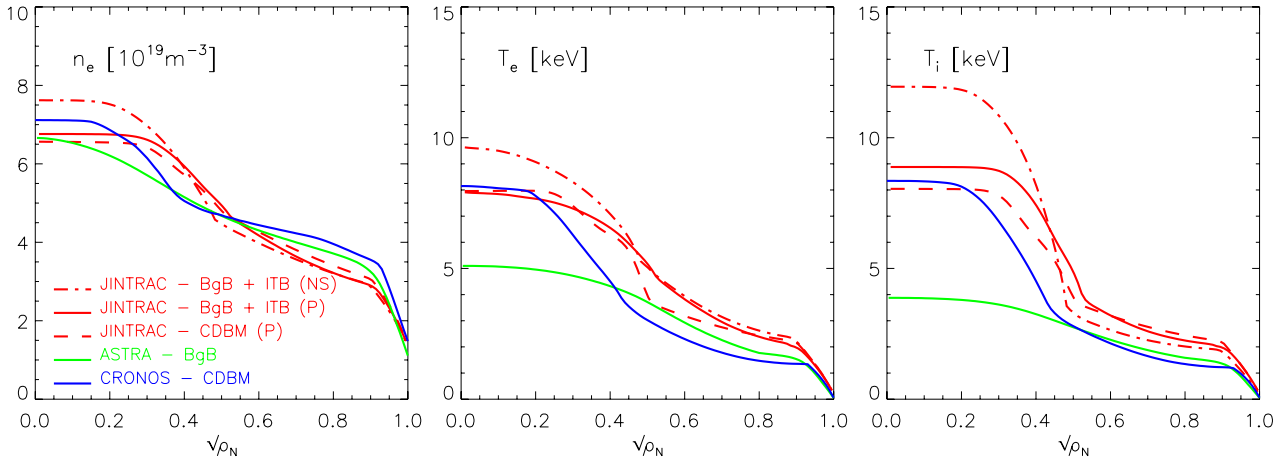

Figure 11. Predicted electron density, electron temperature and ion temperature profiles for a JT-60SA advanced steady-state plasma (scenario 5.1 'high power' version). The codes and the transport models used in the simulations are indicated in the legend (NS and *P* indicates that the beam deposition profiles are obtained from NEMO/SPOT and PENCIL respectively).

Table 3. Reference 0-dimensional parameter for scenario 5.1 ('high power' version) compared with the values obtained from the 1.5-dimensional transport simulations described in the paper.

Scenario 5.1	ASTRA	CRONOS	JINTRAC CDBM / BgB	Reference
B_T (T)	1.72	1.72	1.72 / 1.72	1.72
I_p (MA)	2.3	2.3	2.6 / 2.7	2.3
f_{bs} (%)	53	67	78 / 78	68
f_{ni} (%)	87	106	110 / 110	100
q_{95}	6.6	6.5	5.8 / 5.5	5.8
P_{NBI} (MW)	31	29	30 / 30	30
P_{ECRH} (MW)	7.0	7.0	7.0 / 7.0	7.0
n_{e0} (10^{19} m^{-3})	6.7	7.0	6.6 / 6.8	6.6
$\langle n_e \rangle$ (10^{19} m^{-3})	4.2	4.4	4.3 / 4.3	4.2
T_{e0} (keV)	5.1	8.0	8.0 / 7.9	6.7
$\langle T_e \rangle$ (keV)	2.8	3.0	3.8 / 4.0	3.3
T_{i0} (keV)	3.9	8.2	8.0 / 8.9	7.1
$\langle T_i \rangle$ (keV)	2.2	3.0	3.8 / 4.1	3.4
W_{th} (MJ)	7.2	9.0	10.8 / 11.8	8.4
H_{98}	1.0	1.8	1.2 / 1.2	1.3
β_N	3.9	4.7	5.2 / 5.5	4.3
τ_E (s)	0.19	0.25	0.31 / 0.33	0.31
Z_{eff}	2.0	2.0	1.7 / 1.7	—

As for the previous scenarios, the 0-dimensional parameters derived from these simulations are summarized in table 3 (apart from the results from the JINTRAC simulation with NBI deposition from NEMO/SPOT), where the reference values are also reported for comparison. Also in this case it can be seen that, despite the differences in the density and temperature profiles predicted by the different codes, in general all codes give values for 0-dimensional quantities close to the reference. In particular the bootstrap fraction of the total current f_{bs} is between 60% and 80% in all cases predicting the existence of an ITB. In the JINTRAC simulations the combined current drive resulting from the strong ITB driving a significant amount of bootstrap current and the high NBI power results in a total plasma current above the nominal value for this scenario of 2.3 MA. Moreover, the value of β_N in the JINTRAC simulation is significantly higher than in the other simulations due to the strength of the ITB. It is also interesting to note that even in a case without ITB the ASTRA simulation predicts for this scenario $f_{bs} > 50\%$.

5.2. Steady-state H-mode scenario: 'low power' version

For the analysis of the 'low power' version of scenario 5.1 we performed two JINTRAC runs similar to those executed for the 'high power' version of the scenario.

The first run is a fully predictive simulation where we solved the equations for the current, the density, the ion and electron temperature and the toroidal rotation using the Bohm/gyro-Bohm transport model with the inclusion of an ITB, as described in the previous subsection. The second run was a semi-predictive JINTRAC simulation where we prescribed the same the density profile used in TOPICS and solved the equations for the current and the ion and electron temperature. In this simulation we used the CDBM transport model for heat transport. It should be noted that, in this second simulation, we used the CDBM transport model in the region $\rho \leqslant 0.8$ and prescribed a fixed value for $\chi_{e,i}$ for $0.8 < \rho \leqslant 1$ in order to approach at $\rho = 0.8$ the ion and electron temperature that TOPICS obtains by imposing the boundary conditions at $\rho = 0.85$.

In both cases the power deposition, current drive and torque profile associated with the beam injection were calculated self-consistently by PENCIL inside JINTRAC. The prescription for the current density profile associated with the ECCD was the same as in the 'high power' simulations. In this way we were able to test the sensitivity of the ITB formation to the transport model and of the q profile to the details of the beam power deposition, current drive and torque profile.

The results are summarized in figures 12–14. In figure 12 and 13 we show the total current density profile, the neutral beam-driven current density, the electron cyclotron-driven and the bootstrap current density for the two cases. It can be seen that the peak of the bootstrap and the beam-driven current density profile are displaced towards higher ρ for the

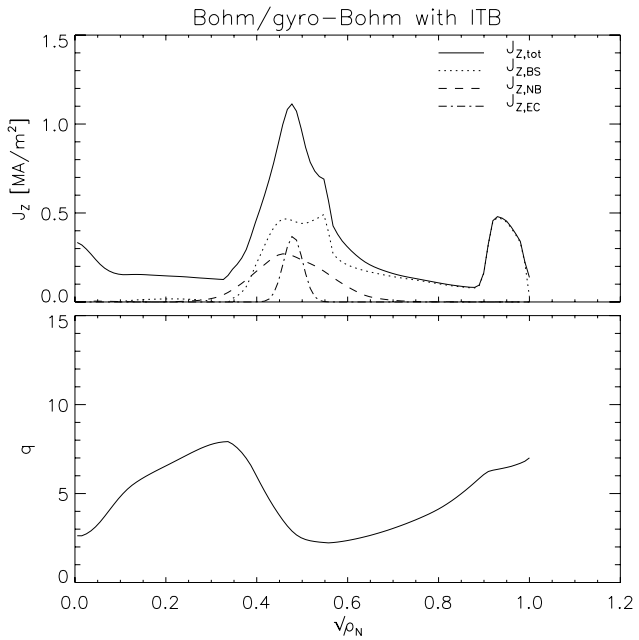

Figure 12. Total current density j_z, neutral beam-driven current density $j_{z,\mathrm{NB}}$, bootstrap current density $j_{z,\mathrm{BS}}$, electron cyclotron driven current density $j_{z,\mathrm{EC}}$ and safety factor q profiles for a JT-60SA advanced steady-state plasma (scenario 5.1 'low power' version). The code used in the simulation is JINTRAC with the Bohm/gyro-Bohm transport model and the neutral beam-driven current density is self-consistently calculated with PENCIL.

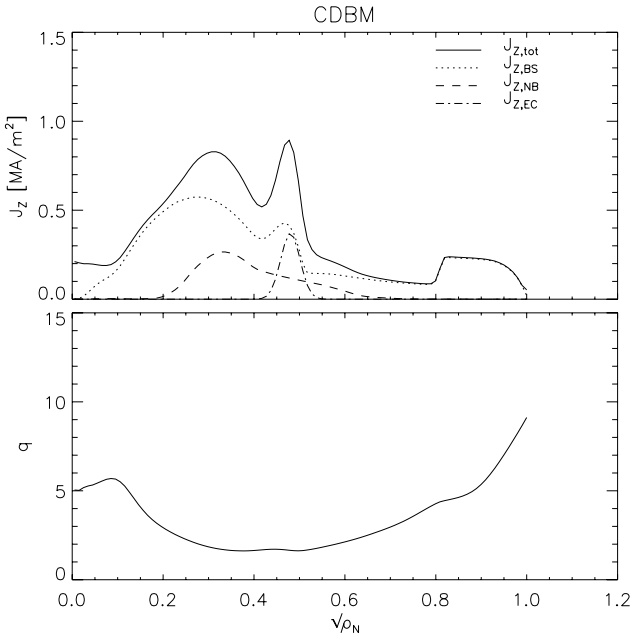

Figure 13. Total current density j_z, neutral beam-driven current density $j_{z,\mathrm{NB}}$, bootstrap current density $j_{z,\mathrm{BS}}$, electron cyclotron driven current density $j_{z,\mathrm{EC}}$ and safety factor q profiles for a JT-60SA advanced steady-state plasma (scenario 5.1 'low power' version). The code used in the simulation is JINTRAC with the CDBM transport model and the neutral beam-driven current density is self-consistently calculated with PENCIL.

Bohm/gyro-Bohm simulation with respect to CDBM. This is due to the fact that, as shown in figure 14, the Bohm/gyro-Bohm transport model predicts a broader density profile compared to CDBM, which causes the beam penetration to be more peripheral. A consequence of this fact is that, although the shape of the beam driven current density profile is similar in the two cases, because of volume effects, the total neutral beam-driven current was ∼0.4 MA in the Bohm/gyro-Bohm case and ∼0.3 MA in the CDBM case. The cumulative effect of these differences is that, for the applied V_{loop}, in the Bohm/gyro-Bohm case it should be possible to drive completely non-inductively the 2.3 MA foreseen for this scenario, whereas the total current obtained in the CDBM case is ≈2.2 MA.

JINTRAC results obtained with the Bohm/gyro-Bohm transport model are in broad agreement with TOPICS results obtained with the CDBM transport model [19] and indicate that scenario 5.1 could achieve a fully non-inductive current of 2.3 MA. This is not the case for JINTRAC simulations with the CDBM transport model, which show that the low power version of scenario 5.1 may not be achieved completely non-inductively. This difference may be caused by the residual difference of pedestal profiles and, if the bootstrap current driven by the ITB remains similar, the lower bootstrap current driven by the ETB. More importantly, it should be noted that one major difference between JINTRAC and TOPICS simulations is that for JINTRAC simulations the total beam-driven current I_{nb} was lower than the one predicted by TOPICS with the CDBM transport model, which was ∼0.5 MA (note that due to the small contribution of the EC driven current to the total current in this scenario, I_{nb} can be approximately estimated as $I_{\mathrm{nb}} \approx I_{\mathrm{p}}(f_{\mathrm{ni}} - f_{\mathrm{bs}})$ using for f_{ni} and f_{bs} the values in table 4).

These results show that, although the existence of an ITB and its radial position and strength may be important to achieve a low-power version of the fully non-inductive scenario 5.1, an equally important role is played by the beam-driven current and the feasibility of the scenario depends crucially on the NBI driving enough current.

The density and temperature profiles obtained with the different codes and transport models are shown in figure 14. As stated above, JINTRAC predicts the formation of a somewhat wider ITB ($\rho \approx 0.6$) with the Bohm/gyro-Bohm model than with the CDBM model ($\rho \approx 0.4$). The result of JINTRAC with the Bohm/gyro-Bohm model is close to the one of TOPICS with CDBM insofar both models predict the formation of an ITB at the same location ($\rho \approx 0.6$). However, JINTRAC gives a suppression of heat conductivity only locally, whereas TOPICS indicates that the heat transport is suppressed to or below the ion neoclassical level inside the ITB. For this reason the two codes give different predictions for on-axis T_{e} and T_{i}.

In figure 14 we plot also the result of a CRONOS simulation where the density profile was prescribed as in the TOPICS simulation and the CDBM transport model was used to predict the ion and electron temperature. The resulting temperature profiles are similar to the JINTRAC results (closer to the ones obtained with the Bohm/gyro-Bohm model for the electron temperature and with the CDBM model for the ion temperature).

Finally, it is worth mentioning that the difference in the location of the ITB between the simulation with JINTRAC and CDBM and the simulations with CRONOS and TOPICS with CDBM is due to the different shape of the q profile and the strong sensitivity of the CDBM transport model to

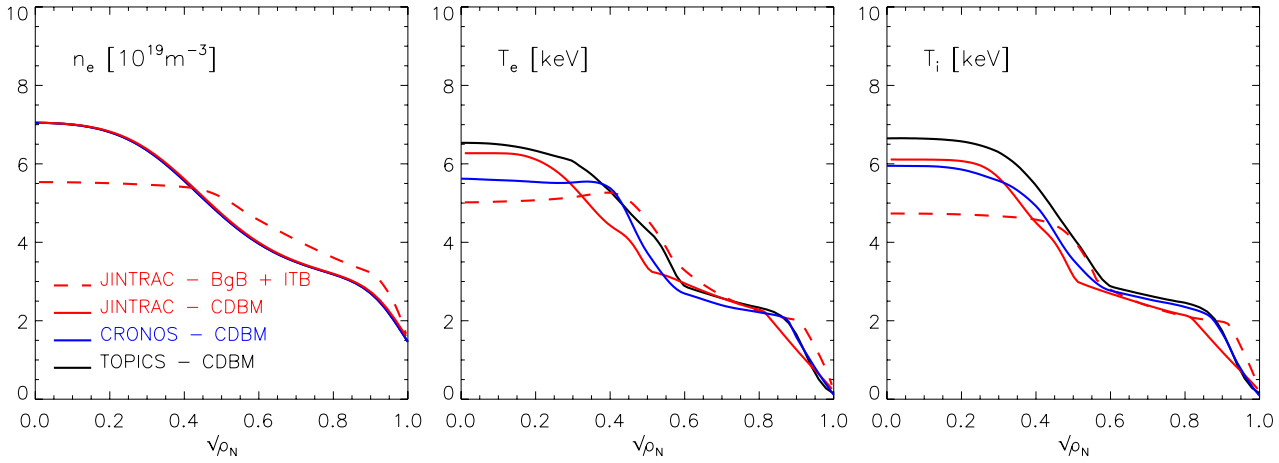

Figure 14. Predicted electron density, electron temperature and ion temperature profiles for a JT-60SA advanced steady-state plasma (scenario 5.1 'low power' version). The codes and the transport models used in the simulations are indicated in the legend.

it. This sensitivity to the q profile highlights the importance of complementing the flat-top simulations presented in this paper with simulations of the current ramp-up and the current profile tailoring in particular when the CDBM model is used. The modelling of the current ramp-up will indicate whether the nominal plasma flat-top parameters can be achieved and what level of control will be necessary to do it. This activity is outside the scope of this paper, but has already started within the EUROfusion JT-60SA work package.

As for the previous scenarios, the 0-dimensional parameters derived from these simulations are summarized in table 4. The result indicate that, in general, despite the differences in the density and temperature profiles predicted by the different codes, all codes give values for 0-dimensional quantities close to each other and that even the 'low power' version of scenario 5.1 should achieve a fully non-inductive steady state. In addition, this 'low power' version of scenario 5.1 would operate at a safer level of β_N, in order to avoid MHD instabilities. However, this 'scaled-down' version of the scenario is more sensitive to the details of the beam-driven current density profile. In fact, the total beam-driven current might not be sufficient to achieve a fully non-inductive steady-state plasma.

Table 4. 0-dimensional parameter for scenario 5.1 ('low power' version) obtained from the 1.5-dimensional transport simulations described in the paper.

Scenario 5.1	CRONOS	JINTRAC CDBM / BgB	TOPICS
B_T (T)	1.72	1.72 / 1.72	1.72
I_p (MA)	2.3	2.2 / 2.3	2.3
f_{bs} (%)	61	74 / 67	72
f_{ni} (%)	83	91 / 83	94
q_{95}	5.6	6.7 / 6.5	5.4
P_{NBI} (MW)	17	17 / 17	17
P_{ECRH} (MW)	7	7 / 7	7
n_{e0} (10^{19} m^{-3})	7.0	7.0 / 5.5	7.1
$\langle n_e \rangle$ (10^{19} m^{-3})	4.1	4.1 / 4.2	4.1
T_{e0} (keV)	5.6	6.2 / 5.0	6.5
$\langle T_e \rangle$ (keV)	3.2	3.0 / 3.3	3.3
T_{i0} (keV)	5.9	6.1 / 4.7	6.7
$\langle T_i \rangle$ (keV)	3.2	2.9 / 3.0	3.4
W_{th} (MJ)	8.0	8.0 / 8.0	9.0
H_{98}	1.5	1.2 / 1.2	1.5
β_N	3.7	3.7 / 3.5	3.9
τ_E (s)	0.33	0.33 / 0.38	0.37
Z_{eff}	2.0	2.0 / 2.0	2.0

6. Discussion

The simulations described in the previous sections aimed at assessing the sensitivity of the general performance of three of the main operational scenarios envisaged for JT-60SA to the physical assumptions on the core transport model and the behaviour of the pedestal. To this purpose we used different codes equipped with semi-empirical and physics-based transport models and making different assumptions on the height and the width of the density and temperature pedestal and compared the results between them and with the reference 0-dimensional values.

The main indication emerging from the set of simulations performed is that, if the properties of the H-mode pedestal are similar, the variability in the main 0-dimensional parameters for each scenario due to the use of different core transport models remains within 30–40% even though the local differences in the density and temperature profiles can be significant (up to 70%). Moreover, the 0-dimensional parameters obtained from the transport simulations described in this paper are in good agreement with the reference values in the research plan and give confidence on the robustness of the scenarios with respect to variations of the details of the radial profiles.

Particular care should be used in the modelling of the advanced steady-state scenario. All codes predict the formation of an ITB, but its strength and location vary from code to code. For the 'high power' version of the scenario, these differences do not influence dramatically the predicted 0-dimensional parameters of the scenario, indicating that, thanks to the strong bootstrap current driven by the ITB and the current density associate with the high neutral beam power, such a scenario should be achievable independently of the fine details of the profile of the non-inductively driven current density.

However, the 'low power' version of the scenario is more sensitive to the details of the bootstrap and beam-driven current density profile. Indeed, one would expect that with less beam power available the tailoring of the deposition profile becomes comparatively more critical.

Moreover, it is important to note that both from the point of view of predicting the total stored energy and the global plasma performance and from the point of view of assessing the feasibility of a steady-state fully non-inductive plasma scenario it is essential to accurately model the characteristic of the density and temperature pedestal. Unfortunately, this is an area where there are fewer and less reliable models available with respect to the core transport and significant effort will be required to reach a level of reliability of the simulations sufficient to reduce the uncertainty associated with this aspect of the scenario modelling.

Finally, given that one of the missions of JT-60SA will be to explore and prepare scenarios for Demo, it should be pointed out that, although the predictions of the different codes for the general performance of the D-D scenario analysed are similar, the differences may become significant when extrapolating to D-T. Relatively small differences in the predicted T_i profiles, for example, could be amplified and lead to considerably different results in terms of fusion performances and neutron yield. In this sense JT-60SA will play an important role in helping discriminate between different transport models.

7. Conclusions

In this paper we have presented simulations of the flat-top phase of the main JT-60SA operational scenarios performed with different codes and transport models. The results have been compared with the predictions of simpler codes featuring only a simplified description of the transport properties of the plasma.

The results show that, although the details of the kinetic profiles may differ from code to code, within the range of codes employed in the simulations, the results of the one-dimensional simulations are in line with the projected scenarios. The degree of variability between the prediction of the different transport models is within 30% for the most important zero-dimensional plasma parameters. The only caveat comes from the fully non-inductive steady-state scenario. Our simulations indicate that the feasibility of the low-power version of this scenario could depend crucially on the details of the beam-driven current density profile.

Nevertheless, it is important to stress that the above conclusions are true when the codes are tuned against each other to replicate similar density and temperature pedestal characteristics (i.e. width and height). Different assumptions on the pedestal performance could lead to significantly different predictions even when using the same core transport model. Therefore it is important to develop a reliable model capable to predict the behaviour of the density and temperature pedestal and integrate it into the core transport simulations. Such a task, however, is beyond the scope of this paper.

On a shorter time scale, although the pedestal pressure gradients assumed in the simulations for the three scenarios appear to be below the peeling-ballooning stability limit, it would be important to analyse the stability properties of the pedestal profiles with state-of-the-art stability codes. This activity, together with the analysis of the time dependent phases of the scenarios (i.e. current ramp-up and ramp-down) is planned within the EUROfusion JT-60SA work package.

Finally, it should be noted, however, that more significant differences between predictions obtained with different codes may appear in the extrapolation from the scenarios presented in this paper to D-T plasmas, where the neutron yield will vary more significantly between different simulations, or to a metal divertor, where the accumulation of heavy impurities (not simulated in the present study) will depend critically on the details of the kinetic profiles [41].

Acknowledgments

This work has been carried out within the framework of the EUROfusion Consortium and has received funding from the Euratom research and training programme 2014–2018 under grant agreement No 633053 and from the RCUK Energy Programme (grant number EP/P012450/1). The views and opinions expressed herein do not necessarily reflect those of the European Commission.

The authors gratefully acknowledge members of the JT-60SA Integrated Project Team for data exchange and fruitful discussions.

ORCID iDs

L. Garzotti https://orcid.org/0000-0002-3796-9814
J. Garcia https://orcid.org/0000-0003-0900-5564

References

[1] JT-60SA Research Plan, version 3.3 www.jt60sa.org/pdfs/JT-60SA_Res_Plan.pdf (March 2016)
[2] Tani K., Azumi M. and Devoto R.S. 1992 *J. Comput. Phys.* **98** 332
[3] Artaud J.F. *et al* 2005 *32nd European Physical Society Conf. on Plasma Physics and Controlled Fusion Combined with the 8th Int. Workshop on Fast Ignition of Fusion Targets (Tarragona, Spain, 27 June–1 July 2005) (Europhysics Conf. Abstracts* vol 29C) ed C. Hidalgo and B.P. van Milligen (Mulhouse: European Physical Society) P1.035 (http://epsppd.epfl.ch/Tarragona/pdf/P1_035.pdf)
[4] Giruzzi G., Artaud J.F., Joffrin E., Garcia J., Ide S., JT-60SA Research Plan Contributors and The JT-60SA Team 2012 *39th European Physical Society Conf. on Plasma Physics and 16th Int. Congress on Plasma Physics (Stockholm, Sweden, 2–6 July 2012) (Europhysics Conf. Abstracts* vol 36F) ed S. Ratynskaya *et al* (Mulhouse: European Physical Society) P5.018 (http://ocs.ciemat.es/epsicpp2012pap/pdf/P5.018.pdf)
[5] Garcia J., Hayashi N., Baiocchi B., Giruzzi G., Honda M., Ide S., Maget P., Narita E., Schneider M., Urano H. and The JT-60U Team, The JET EFDA Contributors and The

EU-ITM ITER Scenario Modelling Group 2014 *Nucl. Fusion* **54** 093010
[6] Boboc A., Gil C., Terranova D., Orsitto F.P., Soare S., Lotte P., Sozzi C., Imazawa R., Kubo H. Feasibility study for a far infrared laser based polarimeter diagnostic system on JT-60SA fusion experiment *Plasma Phys. Control. Fusion* submitted
[7] Bolzonella T. *et al* 2017 *Preprint: 2016 IAEA Fusion Energy Conf. (Kyoto, Japan, 17–22 October 2016)* TH/P1-18 (https://nucleus.iaea.org/sites/fusionportal/Shared%20Documents/FEC%202016/fec2016-preprints/preprint0468.pdf)
[8] Lang P.T., Nakano T., Pégourié B., Ploeckl B. and Sakurai S. 2017 *Fusion Eng. Des.* **123** 167
[9] Romanelli M. *et al* 2017 *Nucl. Fusion* **57** 116010
[10] Romanelli M. *et al* 2015 *Nucl. Fusion* **55** 093008
[11] Garzotti L. *et al* 2016 *43th European Physical Society Conf. on Plasma Physics (Leuven, Belgium, 4–8 July 2016) (Europhysics Conf. Abstracts* vol 40A) ed P. Mantica *et al* (Mulhouse: European Physical Society) O4.113 (http://ocs.ciemat.es/EPS2016PAP/pdf/O4.113.pdf)
[12] Pereverzev G.V. and Yushmanov P.N. 2002 ASTRA automated system for transport analysis in a tokamak *IPP-Report* 5/98, Max-Planck-Institut fur Plasmaphysik (http://www2.ipp.mpg.de/~git/astra/astra.pdf)
[13] Artaud J.F. *et al* 2010 *Nucl. Fusion* **50** 043001
[14] Romanelli M. *et al* and EFDA-JET Contributors 2014 *Plasma Fusion Res.* **9** 3403023
[15] Hayashi N. and JT-60 Team 2010 *Phys. Plasmas* **17** 056112
[16] Waltz R.E., Staebler G.M., Dorland W., Hammett G.W., Kotschenreuther K. and Konings J.A. 1997 *Phys. Plasmas* **4** 2482
[17] Itoh K., Itoh S.-I., Fukuyama A., Yagi M. and Azumi M. 1994 *Plasma Phys. Control. Fusion* **36** 279
[18] Erba M., Cherubini A., Parail V.V., Springmann E. and Taroni A. 1997 *Plasma Phys. Control. Fusion* **39** 261
[19] Hayashi N., Garcia J., Honda M., Narita E., Ide S., Giruzzi G., Sakamoto Y., The JT-60U Team, The JET Contributors and JT-60SA Research Unit 2017 *Nucl. Fusion* **57** 126037
[20] Staebler G.M., Kinsey J.E. and Waltz R.E. 2005 *Phys. Plasmas* **12** 102508
[21] Bourdelle C., Citrin J., Baiocchi B., Casati A., Cottier P., Garbet X., Imbeaux F. and JET Contributors 2016 *Plasma Phys. Control. Fusion* **58** 014036
[22] Snyder P.B., Groebner R.J., Leonard A.W., Osborne T.H. and Wilson H.R. 2009 *Phys. Plasmas* **16** 056118
[23] Aiba N., Tokuda S., Ishizawa T. and Okamoto M. 2006 *Comput. Phys. Commun.* **175** 269
[24] Parail V. *et al*, JET EFDA Contributors and EU ITM Task Force 2009 *Nucl. Fusion* **49** 075030
[25] Cordey J.G. for the ITPA H-Mode Database Working Group and the ITPA Pedestal Database Working Group 2003 *Nucl. Fusion* **43** 670
[26] Tamor S. 1981 *J. Comput. Phys.* **40** 104
[27] Zagórski R., Giruzzi G., Gałązka K., Ivanova-Stanik I., Romanelli M. and Stępniewski W. 2016 *Nucl. Fusion* **56** 016018
[28] Schneider M., Eriksson L.G., Jenkins I., Artaud J.F., Basiuk V., Imbeaux F., Oikawa T., JET-EFDA Contributors and ITM-TF Contributors 2011 *Nucl. Fusion* **51** 063019
[29] Krivenski V., Fidone I., Giruzzi G., Granata G., Meyer R.L. and Mazzucato E. 1985 *Nucl. Fusion* **25** 127
[30] Challis C.D., Cordey J.G., Hamnen H., Stubberfield P.M., Christiansen J.P., Lazzaro E., Muir D.G., Stork D. and Thompson E. 1989 *Nucl. Fusion* **29** 563
[31] Rome J.A., McAlees D.G., Callen J.D. and Fowler R.H. 1976 *Nucl. Fusion* **16** 55
[32] Mikkelsen D.R. and Singer C.E. 1983 *Nucl. Technol./Fusion* **4** 237
[33] Hamamatsu K. and Fukuyama A. 2001 *Fusion Eng. Des.* **53** 53
[34] Ivanov A.A., Khayrutdinov R.R., Medvedev S.Y. and Poshekhonov Y.Y. 2005 *32nd European Physical Society Conf. on Plasma Physics and Controlled Fusion Combined with the 8th Int. Workshop on Fast Ignition of Fusion Targets (Tarragona, Spain, 27 June–1 July 2005) (Europhysics Conf. Abstracts* vol 29C) ed C. Hidalgo and B.P. van Milligen (Mulhouse: European Physical Society) P5.063 (http://epsppd.epfl.ch/Tarragona/pdf/P5_063.pdf)
[35] Fable E. *et al* and The ASDEX Upgrade Team 2013 *Plasma Phys. Control. Fusion* **55** 124028
[36] Huysmans G.T.A., Goedbloed J.P. and Kerner W. 1991 *Computational Physics: Proc. of the CP90 Europhysics Conf. (Amsterdam, The Netherlands, 10–13 September 1990)* ed A. Tenner (Singapore: Word Scientific) p 371
[37] Cenacchi G. and Rulli M. 1988 Upgrading of an equilibrium-transport Code for a multispecies free-boundary plasma *ENEA Report* RTI/TIB(88)5
[38] Honda M. 2010 *Comput. Phys. Commun.* **181** 1490
[39] Kadomstev B.B. 1975 *Sov. J. Plasma Phys.* **1** 389
[40] Tala T.J.J., Heikkinen J.A., Parail V.V., Baranov Y.F. and Karttunen S.J. 2001 *Plasma Phys. Control. Fusion* **43** 507
[41] Casson F.J. *et al*, JET EFDA Contributors and ASDEX-Upgrade Team 2015 *Plasma Phys. Control. Fusion* **57** 0141031